Electronic Supplementary Information

The Effects of the Reducing Agent on Bottom-Up Au Nanoparticle Mechanosynthesis

Paulo F M de Oliveira,*[a] Adam A L Michalchuk,[b] Julien Marquardt,[b] Torvid Feiler,[b] Carsten Prinz,[b] Roberto M Torresi,[a] Pedro H C Camargo,[a,c] and Franziska Emmerling*[b]

[a]Departamento de Química Fundamental, Instituto de Química, Universidade de São Paulo. Av. Lineu Prestes 748, 05508000, São Paulo, Brazil. E-mail: paulofmo@usp.br

[b]BAM Federal Institute for Materials Research and Testing, Richard-Willstätter-Strasse 11, 12489 Berlin, Germany. E-mail: franziska.emmerling@bam.de

[c]Department of Chemistry, University of Helsinki, A.I. Virtasen aukio 1, Helsinki, Finland.

CONTENTS

S1 Electrochemical Equations

Table S1. Reduction reaction of Au^+ and oxidation reactions and corresponding standard electrochemical potentials of the reducing agent (R_A) reductants used in bottom-up mechanochemical synthesis of Au nanoparticles.

Half-reaction	$\boldsymbol{E^0}$ **(V vs. SHE)***	
$Au^+ + e^- \rightarrow Au^0$	$E^0_{red} = +\,1.830\,V$	(Eq.S1)
Sodium borohydride** – $NaBH_4$ $BH_4^- + 3H_2O \rightarrow B(OH)_3 + 7H^+ + 8e^-$	$E^0_{oxi} = +\,0.481\,V$	(Eq.S2)
Ascorbic Acid – $C_6H_8O_6$ $C_6H_8O_6 \rightarrow C_6H_6O_6 + 2H^+ + 2e^-$	$E^0_{oxi} = -\,0.077\,V$	(Eq.S3)
Hydroquinone – $C_6H_8(OH)_2$ $C_6H_8(OH)_2 \rightarrow C_6H_4O_2 + 2H^+ + 2e^-$	$E^0_{oxi} = -\,0.699\,V$	(Eq.S4)
Sodium citrate – $Na_3C_6H_5O_7$ $C_6H_5O_7^{3-} + 2H_2O \rightarrow 3\,CH_2O + 3\,CO_2 + 3H^+ + 6e^-$	$E^0_{oxi} = -\,1.271\,V$	(Eq.S5)
*Potentials based on the standard hydrogen electrode **in a neutral medium		

According to Table S1, the overall balanced reactions, the cell potential (ΔE^0_{cell}), and variation of free energy of the reaction (ΔG) can be calculated from equations Eq.S6 and S7, respectively. *F* is Faraday's constant (96,485 C.mol^{-1}) and *n* is the number of electrons transferred in the balanced equation (Eq.S8-S11).

$$\Delta E^0_{cell} = E^0_{red} + E^0_{oxi} \qquad \text{(Eq.S6)}$$

$$\Delta G = -nF\Delta E \qquad \text{(Eq.S7)}$$

Table S2. Overall balanced electrochemical reactions for Au^+ reduction with different reducing agents (R_A): $NaBH_4$, Ascorbic acid (AA), Hydroquinone (HQ) and sodium citrate (Ctr) and the corresponding cell potential (ΔE^0_{cell}), number of transferred electrons (n) and the Gibbs free energy for each reaction (ΔG).

$\boldsymbol{R_A}$	**Overall reaction**		$\boldsymbol{\Delta E^0_{cell}\,(V)}$	$\boldsymbol{n}$	$\boldsymbol{\Delta G(kJ.mol^{-1})}$
$NaBH_4$	$8\,Au^+ + BH_4^- + 3\,H_2O \rightarrow 8\,Au^0 + B(OH)_3 + 7\,H^+$	(Eq.S8)	+ 2.311	8	- 1783.8
AA	$2\,Au^+ + C_6H_8O_6 \rightarrow 2\,Au^0 + C_6H_6O_6 + 2\,H^+$	(Eq.S9)	+ 1.753	2	- 338.3
HQ	$2\,Au^+ + C_6H_4(OH)_2 \rightarrow 2\,Au^0 + C_6H_4O_2 + 2\,H^+$	(Eq.S10)	+ 1.131	2	- 218.2
Ctr	$6\,Au^+ + C_6H_5O_7^{3-} + 2\,H_2O \rightarrow 6\,Au^0 + 3\,CH_2O + CO_2 + 3H^+$	(Eq.S11)	+ 0.559	6	- 323.6

Table S3. Overall balanced electrochemical reactions per mol of Au^{+} reduced.

R_A	Reduced Overall reaction per mol of Au^{+}	
$NaBH_4$	$Au^{+} + {}^{1}/_{8}\, BH_4^{-} + {}^{3}/_{8}\, H_2O \rightarrow Au^{0} + {}^{1}/_{8}\, B(OH)_3 + {}^{7}/_{8}\, H^{+}$	(Eq.S12)
AA	$Au^{+} + {}^{1}/_{2}\, C_6H_8O_6 \rightarrow Au^{0} + {}^{1}/_{2}\, C_6H_6O_6 + H^{+}$	(Eq.S13)
HQ	$Au^{+} + {}^{1}/_{2}\, C_6H_4(OH)_2 \rightarrow Au^{0} + {}^{1}/_{2}\, C_6H_4O_2 + H^{+}$	(Eq.S14)
Ctr	$Au^{+} + {}^{1}/_{6}\, C_6H_5O_7^{3-} + {}^{1}/_{3}\, H_2O \rightarrow Au^{0} + {}^{1}/_{3}\, CH_2O + {}^{1}/_{6}\, CO_2 + {}^{1}/_{2}\, H^{+}$	(Eq.S15)

S1.1 – General discussion of the trends of reaction rate and cell potential in solution

Solution-phase bottom-up synthesis of metal particles is known to follow Marcus Theory for electron transfer reactions.[1] It follows that electron transfer reactions in solution follow rates that are proportional to the cell potentials of the red-ox (reductant – precursor) pair.[2] This is exemplified for the reduction of $Au^{III} \rightarrow Au^{0}$, in which the strong reduction power of $NaBH_4$ results in the fastest reduction kinetics[3] when compared with other reducing agents such as hydroquinone[4] or ascorbic acid[5] in certain conditions, for example.[2] It was recently demonstrated that the $Au^{III} \rightarrow Au^{0}$ reduction occurs in two stages, $Au^{III} \rightarrow Au^{I} \rightarrow Au^{0}$, with the second reduction being the rate limiting step.[6] As such, although explicit measurement of the AuCl (Au^{I}) reduction kinetics are not recorded in solution, it follows that they must be consistent with those previously recorded for reduction of Au^{III}. An identical trend correlating the red-ox potential and reaction rates for the reduction of Au^{III} has been also identified for a series of amine reducing agents.[7]

S2 Experimental Protocol

S2.1 Composition of the reactive mixtures

Table S4. Composition of mixtures used for mechanochemical synthesis of gold nanoparticles and their relative amounts.

Reducing agent (R_A)	**R_A (mg)**	**AuCl (mg)**	**AuCl: R_A IMR[a]**	**AuCl:R_A EMR[b]**	**AuCl:R_A mass ratio**	**AuCl mass fraction[c]**	**R_A mass fraction[c]**
$NaBH_4$	2.0	48.6	1:1/8	1:1/4	24.25	0.323	0.013
Ascorbic acid (AA)	21.6	28.5	1:1/2	1:1	1.32	0.190	0.144
Hydroquinone (HQ)	16.1	34.0	1:1.2	1:1	2.11	0.227	0.107
Sodium citrate (Ctr)	15.0	35.2	1:1/6	1:1/3	2.34	0.235	0.100
	19.5	30.5		1:1/2	1.56	0.203	0.130
	28.0	22.0		1:1	0.79	0.147	0.187
	36.0	14.1		1:2	0.39	0.094	0.240

[a]Stoichiometric ratio, according to equations Eq S12-S15 (ESI), to reduce one mol of Au^I. [b]Molar ratio used in the experiments – in all cases the reducing agents were used in excess. [c]Overall mass fraction including PVP (100 mg) + AuCl + R_A.

S2.2 Powder X-ray diffraction (PXRD)

The reduction of AuCl into metallic Au was monitored by PXRD. Following each milling reaction, PXRD patterns were acquired immediately, thereby limiting any effects of aging on the resulting powder samples. PXRD profiles were collected using a Bruker D8 Advance (Bruker AXS GmbH, Germany) diffractometer in Bragg-Brentano geometry using Cu Kα ($\lambda = 1.5406$ Å) with a Ni filter or in a D8 Discover (Bruker AXS GmbH, Germany) diffractometer in transmission mode also with Cu Kα ($\lambda = 1.5406$ Å); For this last, Samples were placed into Lindemann glass capillaries (φ = 0.5 mm) and installed on a rotating sample holder to avoid any artifacts due to preferential orientations of crystallites. Diffraction data were collected over a range of 15-80° 2θ (step width 0.02° 2θ, count time 1 s/step, total collection time 55 min). The effect of aging on the observed composition was found to be negligible, and within the expected experimental errors of our analytical methods. **Figure S1** displays two PXRD profiles collected in immediate succession for the same powder sample. After 55 min (*i.e*. the collection time) the Au^0 content changes by only *ca* 4% (from 0.43 to 0.47).

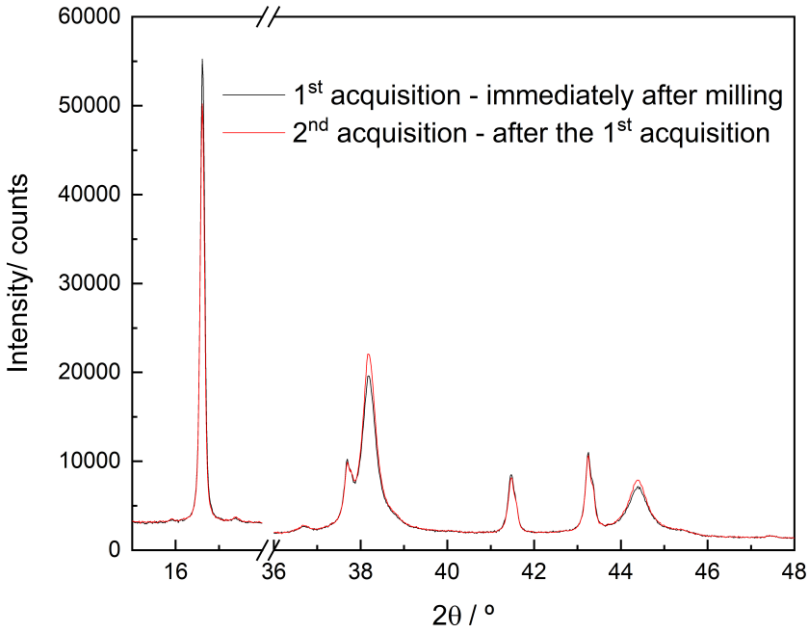

Figure S1. PXRD patterns of the mechanochemical synthesis of AuNPs from the reduction of AuCl by $NaBH_4$. These are subsequent acquisitions to verify aging effects, which was negligible (*ca* 4% in the Au^0 content)

Figure S2 displays the collected XRD patterns for each reducing agent as function of milling time.

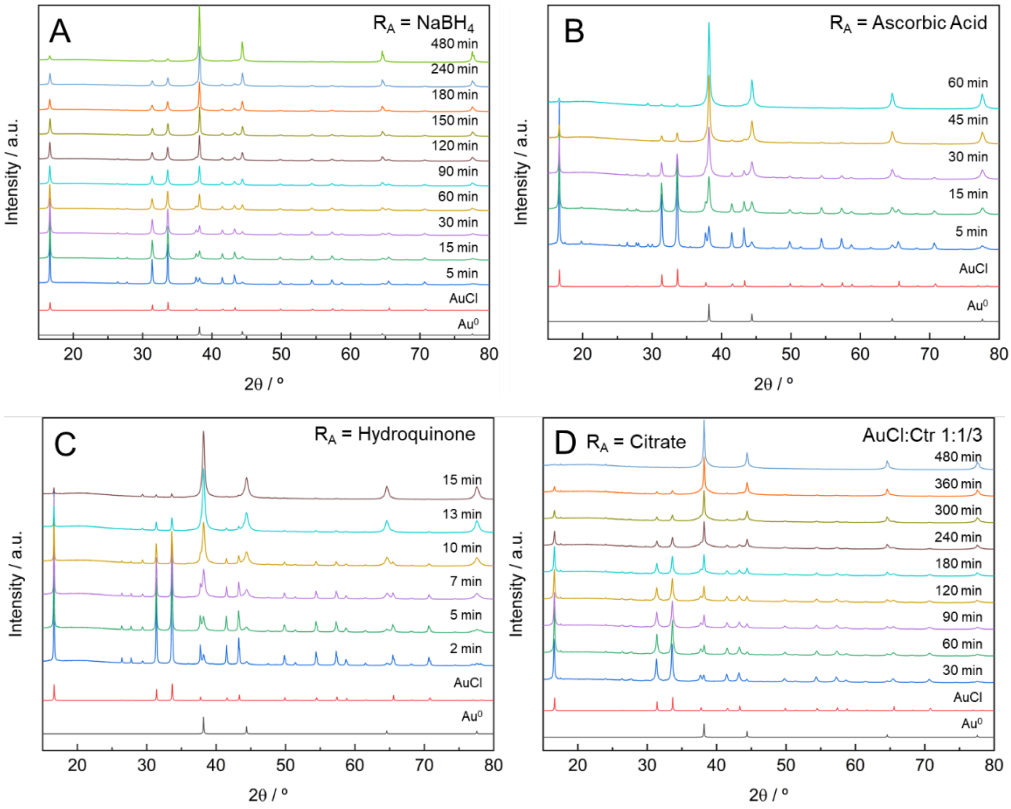

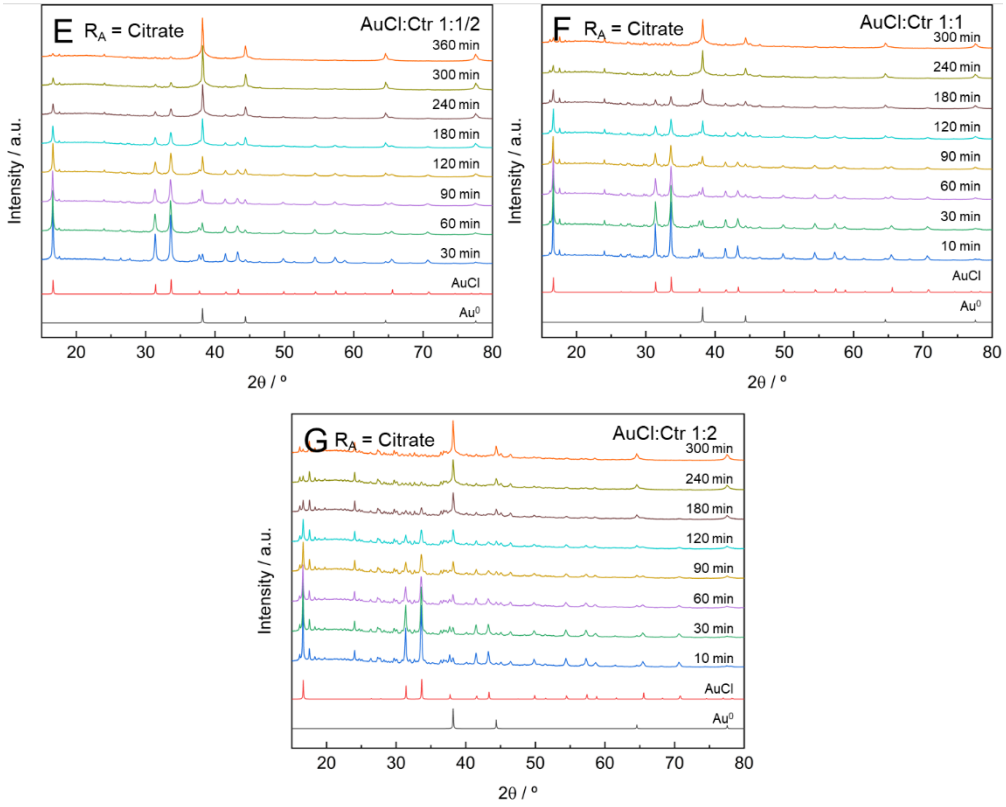

Figure S2. PXRD patterns as function of milling time for Au NP BUMS from the reduction of AuCl by different reducing agents. Simulated Au^0 and AuCl patterns are displayed for comparison. Scattering angles correspond to $\lambda = 1.5406$ Å.

S2.3 Rietveld refinement

Quantitative Rietveld refinements were performed using the FullProf Suite v3.0.0.[8] To account for the influence of the instrument-related peak broadening a LaB_6 standard was measured and treated by full pattern Rietveld refinement. The profile parameters obtained in this way were used to create an instrument resolution function which was considered in each refinement. As starting models for the refinement, gold (ICSD 44362) and gold(I) chloride (ICSD 6052) were applied. A clear bimodal distribution of particle sizes was evident in the powder diffraction profiles as evidenced from the obvious superposition of two dominant reflection line widths**, Figure S3**. To address the bimodal size distribution, refinements were performed by including each phase twice: one modeled with a small domain size (and hence large peak width), and the second with a large domain size (and correspondingly small peak width). **Figure S4** displays the volume fraction of each phase for the case when $NaBH_4$ was used as reducing agent.

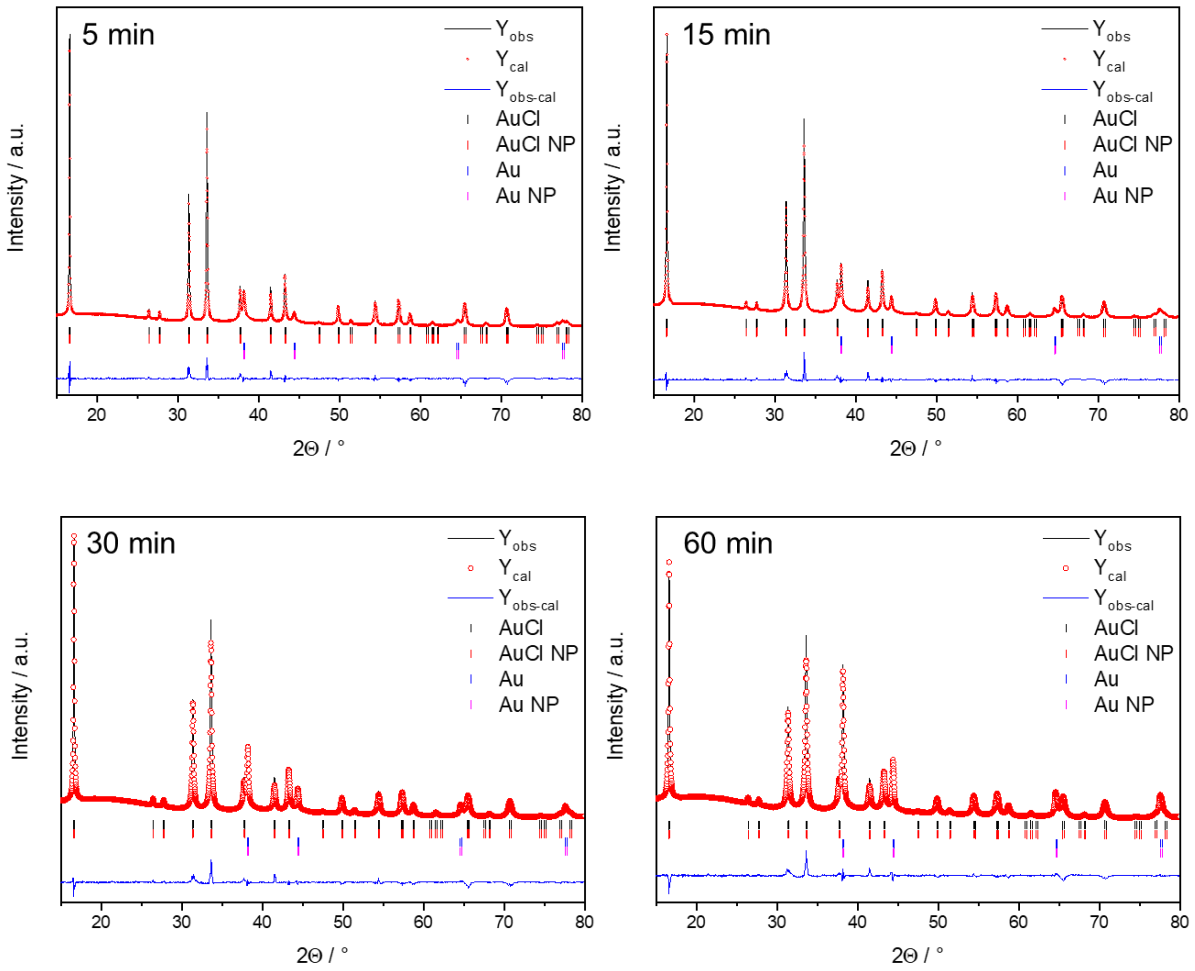
5 min
15 min
30 min
60 min
Y obs
Y cal
Y obs-cal
AuCl
AuCl NP
Au
Au NP
Intensity / a.u.
2Θ / °
20
30
40
50
60
70
80

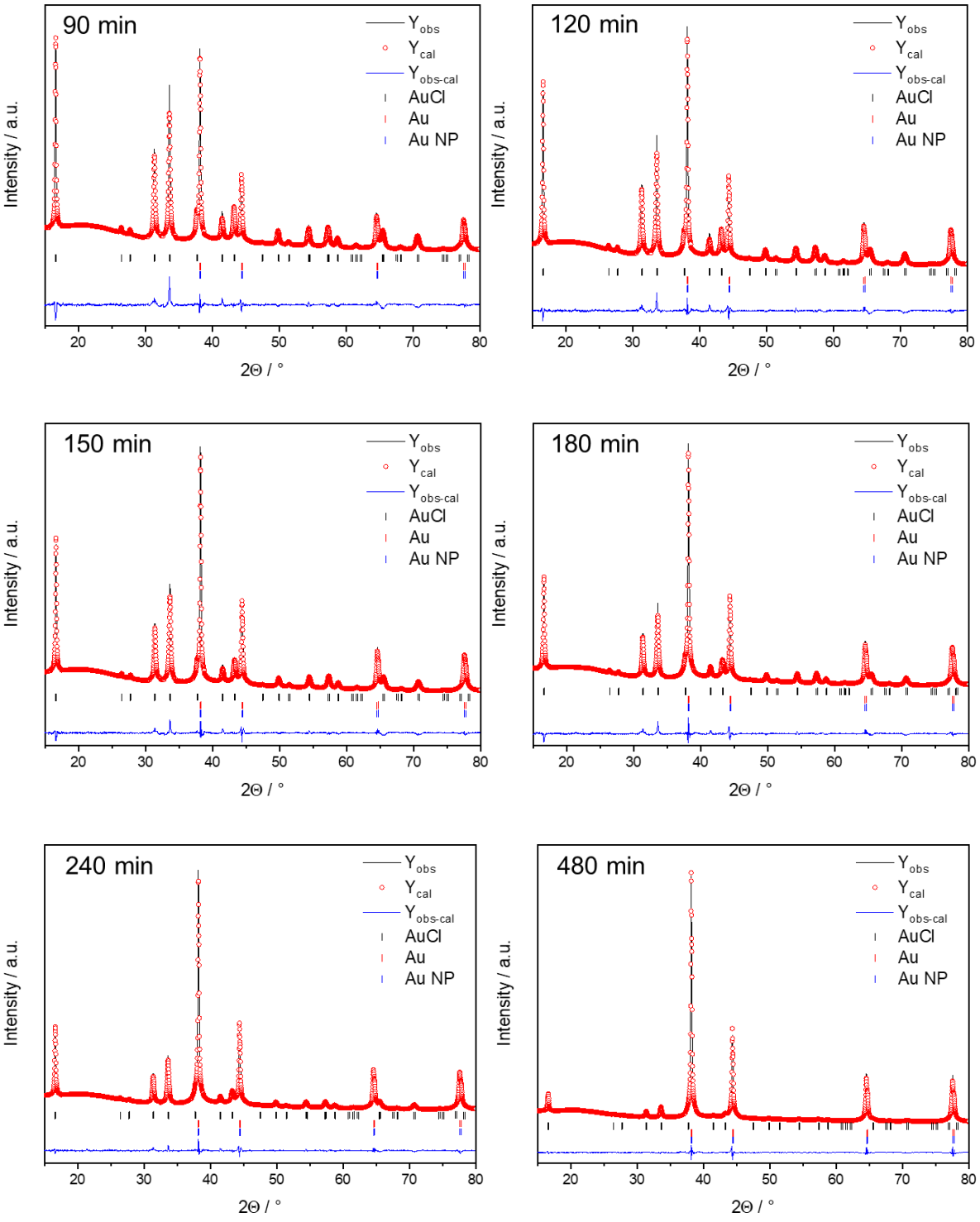

Figure S3. Rietveld refinements for powder diffraction monitoring of AuCl reduction using $NaBH_4$ as reducing agent. The experimental data (black) are shown in each case alongside the fit (red) and difference curves (blue). Tick marks for Bragg reflections corresponding to each phase are shown. Note 'Au' / 'AuCl' correspond to the large domain size Au phase and 'Au NP' / 'AuCl NP' to the small domain size phase (see S2.3 text for discussion). Scattering angles correspond to $\lambda = 1.5406$ Å.

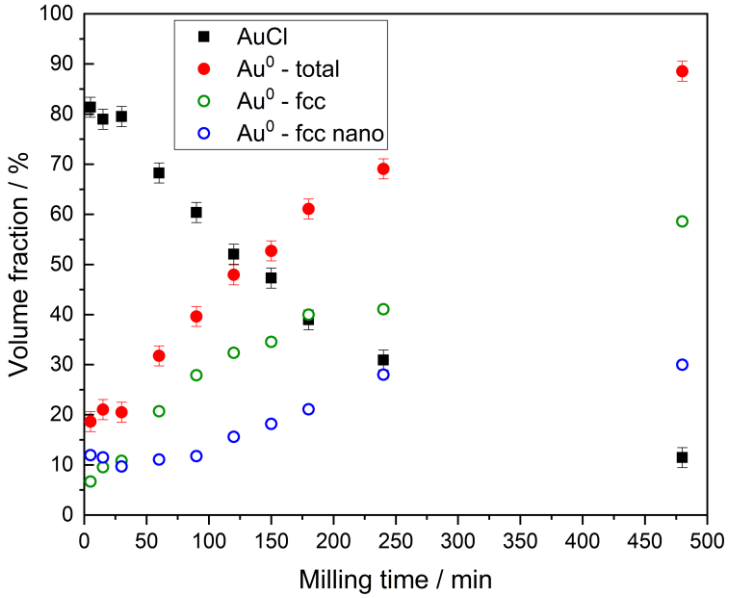

Figure S4. AuCl and Au^0 phase quantification from Rietveld refinement as function of milling time for the bottom-up mechanochemical synthesis of Au NPs using $NaBH_4$ as reducing agent.

S2.4 Integrated peak intensity and calibration

The quality of the data was not always suitable for quantitative Rietveld refinement. Therefore, to facilitate determination of the transformation trends, we correlated the Rietveld quantification of total Au^0 in the $NaBH_4$ run (**Figure S4**) to the ratio of the integrated peak intensities of the main peaks of AuCl ($I_{(011)AuCl}$) and Au^0 ($I_{(111)Au^0}$ or $I_{(200)Au^0}$) phases. To obtain values of $I_{(hkl)}$ the powder diffraction profiles were processed in the HighScorePlus suite (3.0e).[9] The background was fit to a routine polynomial function and subtracted, followed by peak fitting and integration. **Figure S5** shows the correlation curves generated from the Rietveld refinements (**S2.3** and **Figure S4**) against two dominant Bragg reflection intensities from Au^0. These calibration curves were used subsequently to estimate the Au^0 fraction from the ratios of Au/AuCl integrated peak intensities for the runs where hydroquinone, ascorbic acid and sodium citrate were employed as reductants. In **Figure S6**, we can see that both Au^0 integrate peak intensities yield the same trend of transformation.

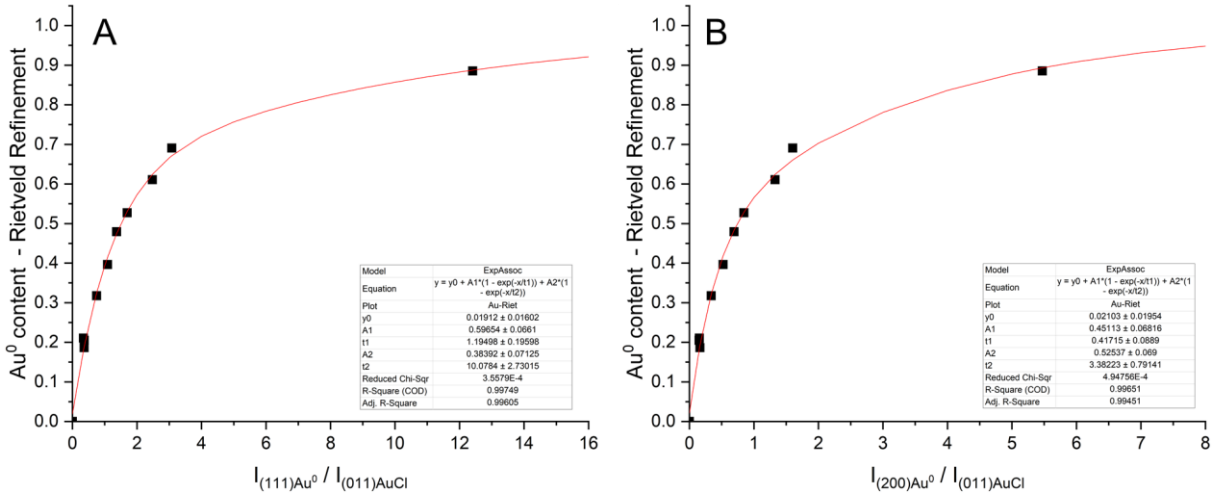

Figure S5. Correlation of Rietveld quantification of total Au^0 and the ratio of the integrated peak intensities of both AuCl and Au^0 phases. The data corresponds to the AuCl reduction using $NaBH_4$. (A) $I_{(111)Au^0}/I_{(011)AuCl}$ and (B) $I_{(200)Au^0}/I_{(011)AuCl}$ ratios.

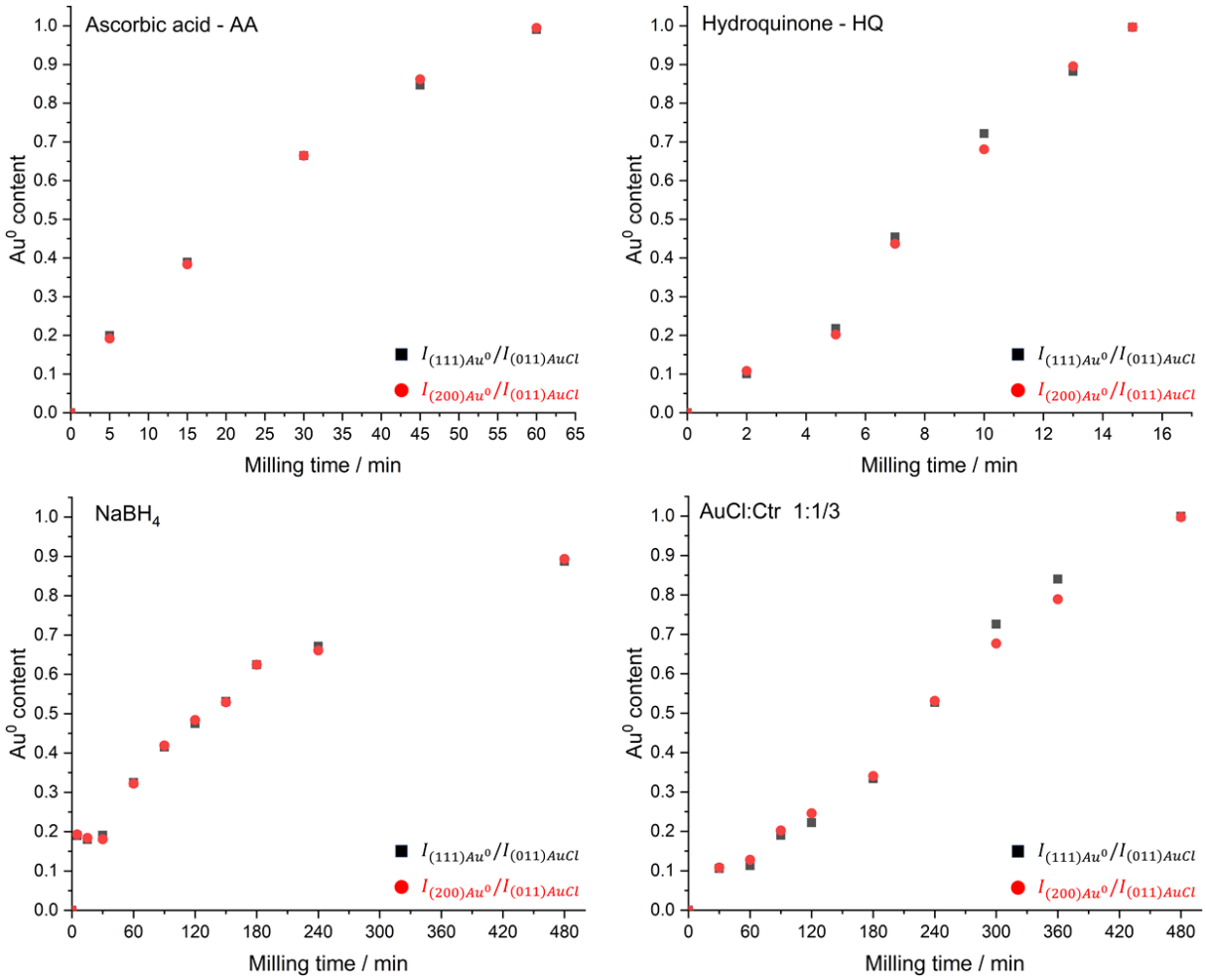

Figure S6. Au^0 content as function of milling time extract according to the correlation curves from Figure S2 for the different reducing agents. Regardless the integrated peak of Au^0 PXRD pattern the same trends are observed.

S2.5 Experimental data fitting

Considering the complexity to determine the elementary steps of ball milling reactions, it is more appropriate to discuss the rate of the transformation in terms of an overall (apparent) rate constant *k'*. Such that the overall macroscopic transformation (α) can be described according to a general equation,

$$\alpha = 1 - e^{(-k' t^n)} \qquad \text{Eq. S16}$$

The form of Equation S16 can fit any profile containing an induction period, an acceleration and a deceleration stage.[10] In the case of Au NP BUMS, an offset (y_0) was included in the equation. This is because at the beginning of the reaction there were already traces of Au^0 from the disproportionation of AuCl during storage (**Figure S7**). Hence, the final form of Eq.S16 used in this work follows as

$$y = y_0 + [1 - e^{(-k' t^n)}] \qquad \text{Eq. S17}$$

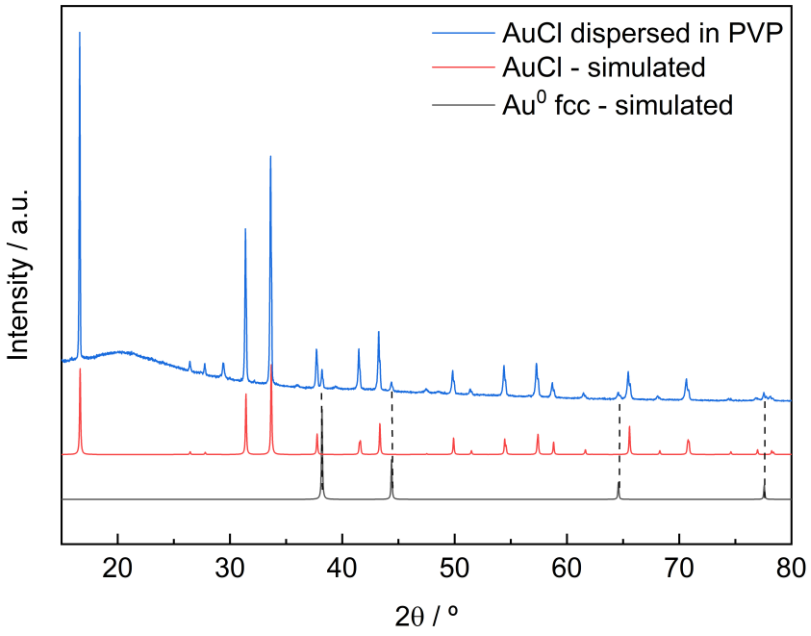

Figure S7. PXRD pattern of AuCl dispersed in PVP (physical mixture). It is possible to detect traces of Au0, resulting from the disproportionation of AuCl[11] during storage. Simulated patterns of AuCl (COD 1510088) and Au (COD 1100138) are also included. Scattering angles correspond to $\lambda = 1.5406$ Å.

The fittings for the experimental data to Eq.S17 are displayed in **Figure S8** for each reducing agent used for the AuCl reduction. When ascorbic acid (AA) or $NaBH_4$ were used as reducing agents we see a monotonic increase in Au NP formation. For these two cases *n* (Equation S17) was refined near unity. When hydroquinone (HQ) or

sodium citrate (Ctr) were employed, the reaction followed a sigmoidal trend. Fitting with *k'* and *n* as free parameters, *n* approached to 2 in all cases (**Figure S8C-G**). Therefore, for a rationale comparison of the rate constants for the citrate concentration studies, we fixed *n*=2. We do not attempt to extract meaningful mechanistic information from these obviously different values of *n* in the different reducing agents in this work. However, it does suggest that there may be important differences between the modes of action of these reducing agents under BUMS conditions, and warrants follow up investigation.

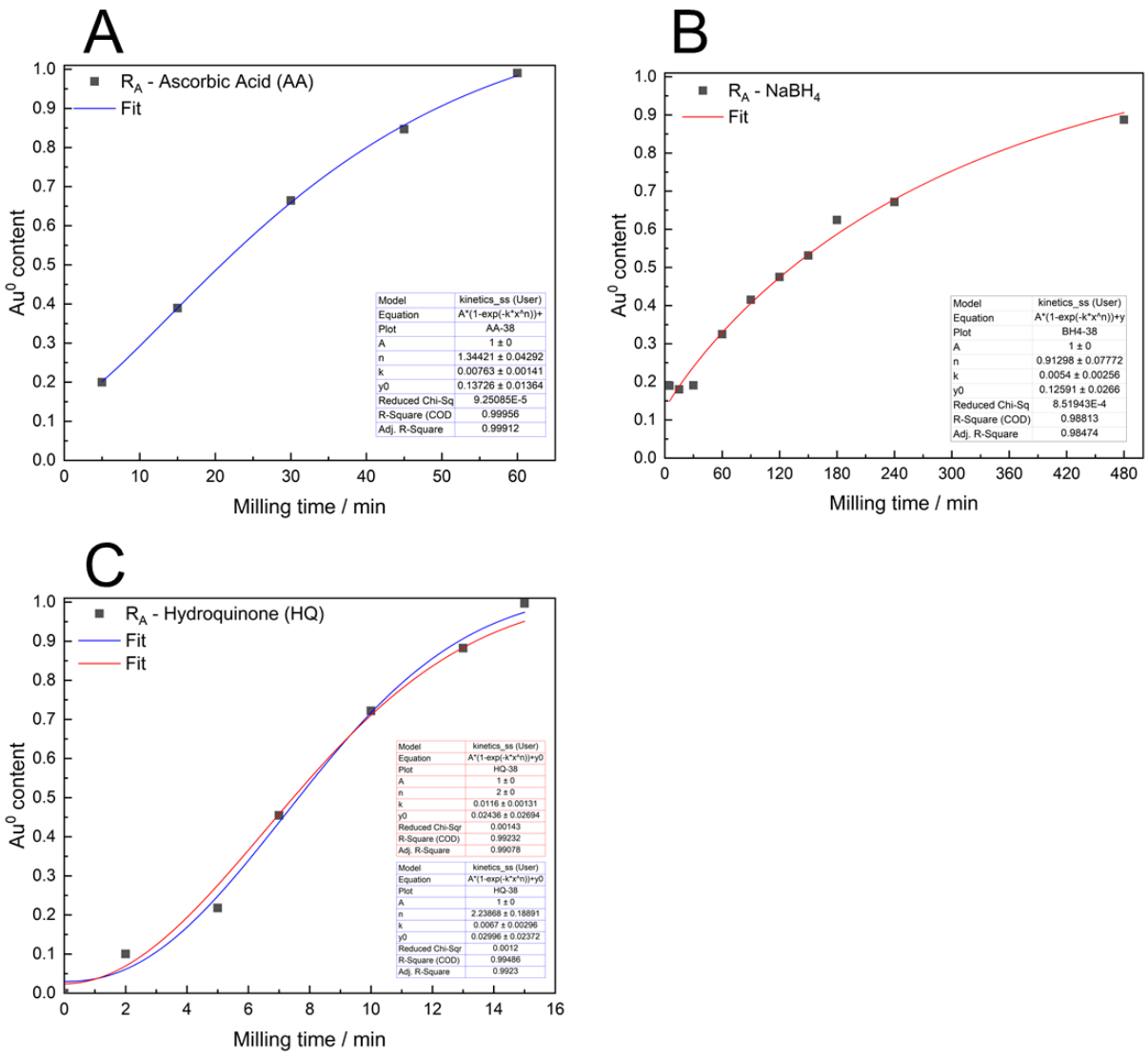

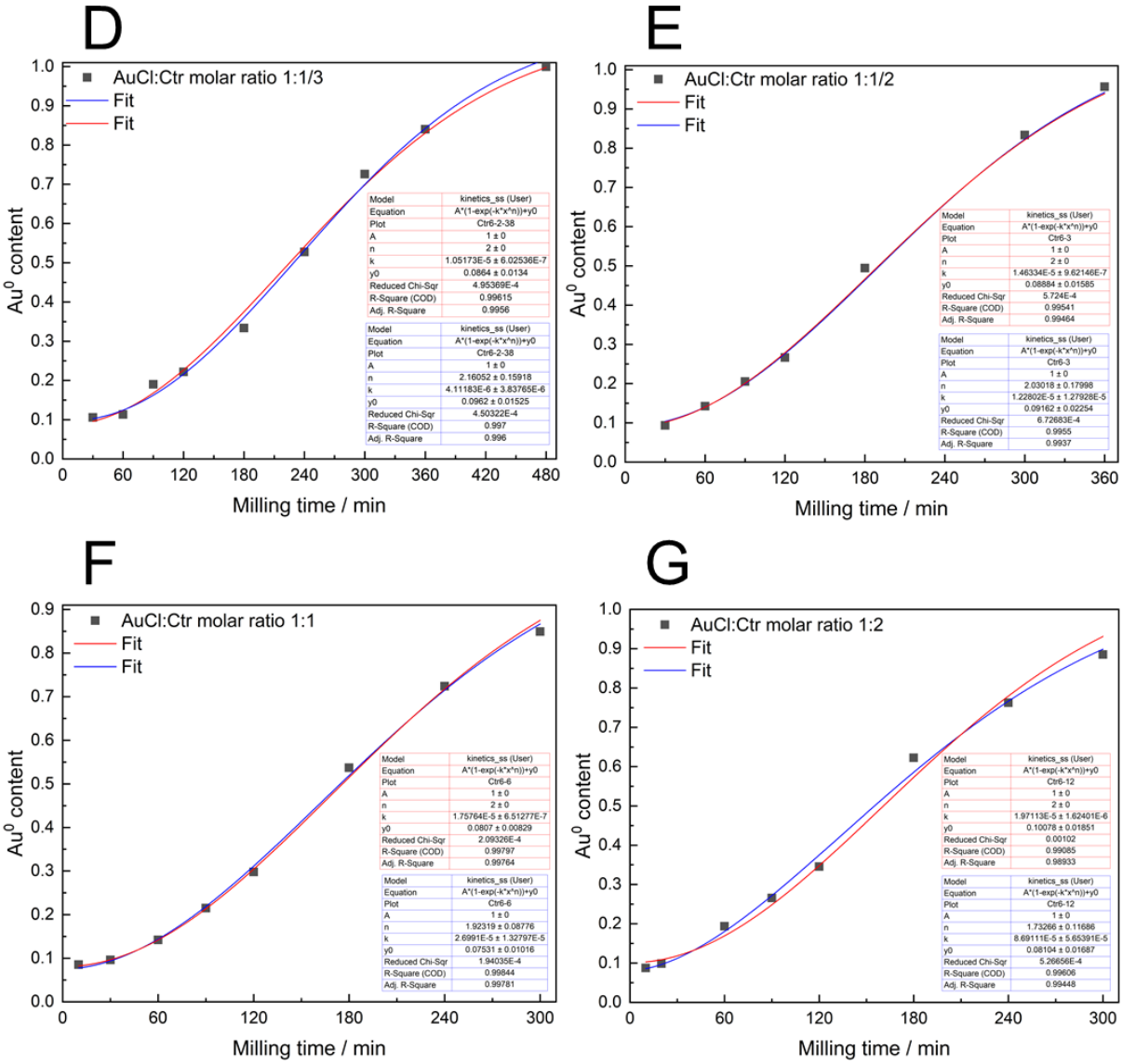

Figure S8. Fits of Equation S17 to the experimental data for the BUMS of AuNPs using (A) Ascorbic acid – AA, (B) $NaBH_4$, (C) Hydroquinone – HQ and (D-G) sodium citrate (Ctr) as reducing agents. From D to G, AuCl:Ctr molar ratio corresponds to 1:1/3, 1:1/2, 1:1 and 1:2, respectively.

S2.6 Particle size distribution

TEM was used for AuNPs imaging. Particle size was measured using ImageJ version 1.52a.[12] For the particle size distribution histograms at least 200 particles were counted.

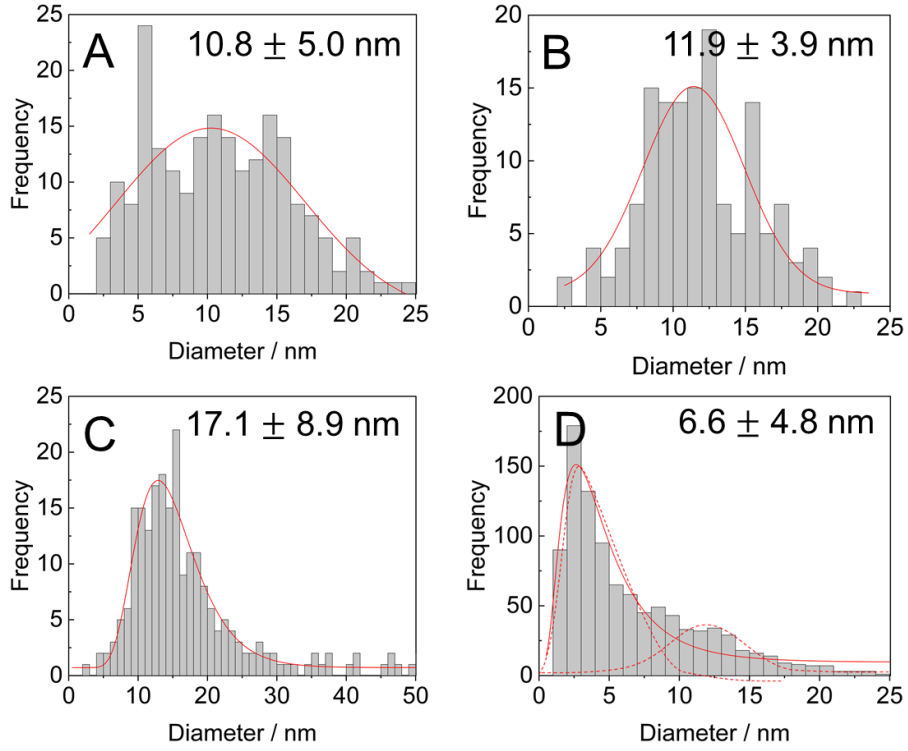

Figure S9. Particle size distribution of AuNPs synthesized using (A) $NaBH_4$, (B) Ascorbic acid (AA), (C) Hydroquinone (HQ) and (D) Sodium Citrate (Ctr) (AuCl:Ctr molar ratio 1:1/3) as reducing agents.

S3 References

1 R. A. Marcus, *Rev. Mod. Phys.*, 1993, **65**, 599–610.

2 T. S. Rodrigues, M. Zhao, T. Yang, K. D. Gilroy, A. G. M. da Silva, P. H. C. Camargo and Y. Xia, *Chem. – A Eur. J.*, 2018, **24**, 16944–16963.

3 J. Polte, R. Erler, A. F. Thünemann, S. Sokolov, T. T. Ahner, K. Rademann, F. Emmerling and R. Kraehnert, *ACS Nano*, 2010, **4**, 1076–1082.

4 L. Vigderman and E. R. Zubarev, *Chem. Mater.*, 2013, **25**, 1450–1457.

5 C.-H. Kuo and M. H. Huang, *Langmuir*, 2005, **21**, 2012–2016.

6 Y. Gao and L. Torrente-Murciano, *Nanoscale*, 2020, **12**, 2740–2751.

7 J. D. S. Newman and G. J. Blanchard, *Langmuir*, 2006, **22**, 5882–5887.

8 J. Rodriguez-Carvajal, *Full Prof suite 3.0.0, Lab. Leon Brillouin, CEA-CNRS, 2003*.

9 T. Degen, M. Sadki, E. Bron, U. König and G. Nénert, *Powder Diffr.*, 2014, **29**, S13–S18.

10 A. A. L. Michalchuk, I. A. Tumanov, S. Konar, S. A. J. Kimber, C. R. Pulham and E. V. Boldyreva, *Adv. Sci.*, 2017, **4**, 1700132.

11 X. Lu, H.-Y. Tuan, B. A. Korgel and Y. Xia, *Chem. - A Eur. J.*, 2008, **14**, 1584–1591.

12 C. A. Schneider, W. S. Rasband and K. W. Eliceiri, *Nat. Methods*, 2012, **9**, 671–675.